Nanoparticle Knudsen layers in gas-filled microscale geometries

M. A. Gallis, J. R. Torczynski,* and D. J. Rader
Engineering Sciences Center, Sandia National Laboratories, P.O. Box 5800, Albuquerque, New Mexico 87185-0346, USA
(Received 5 November 2007; revised manuscript received 17 January 2008; published 5 March 2008)

Nanoparticles suspended in ambient air within microscale geometries form a Knudsen layer when diffusing in a Brownian fashion toward a solid wall. More specifically, the particle number density adjacent to the wall approaches a nonzero value proportional to the flux. An approximate theory for the coefficient of proportionality as a function of the particle sticking fraction at the wall and the drift velocity normal to the wall is compared to Langevin particle simulations. The resulting boundary condition enables accurate advection-diffusion simulations of nanoparticle-aerosol transport.

DOI: 10.1103/PhysRevE.77.036302 PACS number(s): 05.40.Jc, 51.20.+d, 81.07.Wx, 85.85.+j

I. INTRODUCTION

In theoretical treatments of aerosol transport, the particle number density adjacent to a solid boundary (a "wall") is almost universally considered to be zero [1]. While an excellent approximation for micron-scale aerosol particles in ambient air or a similar gas, this assumption breaks down for atmospheric aerosols of nanoparticles now used in experiments [2]. Rather than vanishing at a wall, the particle number density approaches a nonzero value proportional to the particle flux to the wall even when the probability that an impacting particle sticks is unity. The presence of the wall modifies the particle velocity distribution function from its form in an unbounded medium within a few thermal stopping distances of the wall. This affected region is referred to herein as the "particle Knudsen layer" by analogy to the Knudsen layer observed for gas molecules within a few mean free paths of a solid or liquid surface [3,4]. The particle Knudsen layer is investigated theoretically via the generalized Fokker-Planck equation [5] and computationally via massively parallel Langevin (Brownian) particle transport simulations [6]. It has been proved that the dynamics of a heavy particle surrounded by light gas molecules is described by these mathematically equivalent equations [7].

The interaction of a particle with a wall is a highly complicated process and remains the subject of research. In his pioneering experiments involving polystyrene latex (PSL) particles incident on quartz surfaces either in vacuum or with gas present, Dahneke [8] shows that the probability of an impacting particle sticking to a wall typically depends on the particle velocity. Generally, slower particles are more likely to stick, and faster particles are more likely to bounce. At speeds near the crossover from sticking to bouncing, the experimental observations can be approximately correlated by a theoretical expression based on assuming that the particle-wall binding energy and the coefficient of restitution are independent of the particle velocity. However, if the binding energy is treated as an adjustable parameter in the theory, the values from fitting the theory to the measurements are roughly 1000 times larger than values based on van der Waals forces. Moreover, at higher speeds, the coefficient of restitution is observed to be velocity-dependent. This behavior apparently results from processes such as plastic deformation of the particle or the wall, transformation of kinetic energy into heat by internal friction, and radiation of energy away from the impact site by surface or bulk waves in the solid. The presence of gas introduces a further complication in that the fluid drag on a particle depends on the distance to the wall. This phenomenon is well understood for a continuum incompressible fluid. For example, when the particle-wall separation equals the particle radius, the drag roughly doubles [9]. When noncontinuum mean-free-path effects become important (as for nanoparticle aerosols), this phenomenon is not well understood although slip may reduce its importance. Other issues that increase the complexity of the particle-wall interaction process include gas compressibility, surface roughness, deposited or adsorbed material on the surface, the charge state of the particle, and the probability distribution of particle velocities following reflection.

Herein, an idealized system is investigated that includes the important physics but avoids the complexity and empiricism associated with real particle-wall interactions. The drag on the particle as it passes through the gas is taken to be independent of the particle-wall separation, which is accurate until the separation becomes small. If a particle does not stick and thus reflects, the reflection is taken to be specular. Two reflection processes are considered. In the first, a velocity-independent sticking fraction is prescribed, and any particle impacting the wall has this probability of sticking regardless of its incident velocity. In the second, a cutoff velocity is prescribed, and any particle impacting the wall sticks if its normal incident velocity is less than this value. The second process is more physically realistic than the first [8].

II. GENERALIZED-FOKKER-PLANCK APPROXIMATION

An approximate theory for the behavior of particles in the vicinity of a wall can be developed for these two reflection processes. In brief, for a nonzero flux toward the wall, the particle velocity distribution in the gas far from the wall is applied at the wall, and the outgoing portion of the flux is equated to the reflected part of the incoming portion of the flux.

*Corresponding author. FAX: 505-844-6620. jrtorcz@sandia.gov

Chandrasekhar [5] derives the generalized Fokker-Planck equation for the dynamics of a particle in a fluid, Eq. (249) of his treatise, given below in a slightly different notation:

$$\frac{\partial N}{\partial t} + \frac{\partial}{\partial \mathbf{x}} \cdot (\mathbf{u}N) + \frac{1}{\tau}\frac{\partial}{\partial \mathbf{u}} \cdot (-\mathbf{v}N) = \frac{c^2}{2\tau}\frac{\partial}{\partial \mathbf{u}} \cdot \left(\frac{\partial N}{\partial \mathbf{u}}\right). \quad (1)$$

Here, N is the particle velocity distribution function, t is time, $\mathbf{x}$ is position, $\mathbf{u}$ is particle velocity, $\mathbf{v}=\mathbf{u}-\mathbf{U}$ is particle thermal velocity, $c=(2k_BT/m)^{1/2}$ is the most probable particle thermal speed when N is a Maxwellian distribution at temperature T, k_B is the Boltzmann constant, $m=\pi d^3 \varsigma/6$ is the particle mass, d is the particle diameter, ς is the particle mass density, $\mathbf{U}=\mathbf{F}/\beta$ is the drift velocity, $\mathbf{F}$ is the total nondrag force on a particle (e.g., $\mathbf{F}=m\mathbf{g}$ is the force from a gravitational acceleration of $\mathbf{g}$), $\tau=m/\beta$ is the particle stopping time, β is the particle drag coefficient (force per unit velocity), and $D=c^2\tau/2=k_BT/\beta$ is the Stokes-Einstein particle diffusivity [1]. The particle drag coefficient and all quantities derived therefrom depend on the particle properties and the gas conditions. Herein, all particle and gas parameters are taken to be independent of time and position, and the gas is taken to be motionless.

For this situation, the above equation has the following time-independent solution:

$$N = \frac{\tilde{n}}{\pi^{3/2}c^3}\exp\left[-\frac{\mathbf{v}\cdot\mathbf{v}}{c^2}\right], \quad (2)$$

$$\tilde{n} = n_\infty + n_1 \exp\left[\frac{2\mathbf{U}\cdot(\mathbf{x}-\tau\mathbf{v})}{c^2\tau} - \frac{\mathbf{U}\cdot\mathbf{U}}{c^2}\right], \quad (3)$$

$$\tilde{n} \to n_0 + \left(\frac{\partial n}{\partial \mathbf{x}}\right)_0 \cdot (\mathbf{x}-\tau\mathbf{v}). \quad (4)$$

Here, n denotes particle number density, subscripts indicate quantities that are independent of time and position, and the arrow denotes the zero-drift-velocity limit ($\mathbf{U}\to\mathbf{0}$). The zero-drift-velocity solution is physically realizable only in the limit of a small particle-number-density gradient, which ensures that regions of negative probability density occur only at large velocities and thus are exponentially small. This solution possesses the following moments for the particle number density, the particle number flux, the particle energy density, and the particle energy flux, the forms of which can be interpreted in terms of advective transport, diffusive transport, directed kinetic energy, internal energy, and enthalpy, where D is the particle diffusivity, m is the particle mass, k_B is the Boltzmann constant, and T is the temperature:

$$\int N d\mathbf{u} = n = n_\infty + n_1 \exp\left[\frac{\mathbf{U}\cdot\mathbf{x}}{D}\right] \to n_0 + \left(\frac{\partial n}{\partial \mathbf{x}}\right)_0 \cdot \mathbf{x}, \quad (5)$$

$$\int N\mathbf{u}d\mathbf{u} = n\mathbf{U} - D\frac{\partial n}{\partial \mathbf{x}}, \quad (6)$$

$$\int N\left(\frac{1}{2}m\mathbf{u}\cdot\mathbf{u}\right)d\mathbf{u} = \frac{1}{2}m\mathbf{U}\cdot\left(n\mathbf{U} - D\frac{\partial n}{\partial \mathbf{x}}\right) + \frac{3}{2}nk_BT, \quad (7)$$

$$\int N\left(\frac{1}{2}m\mathbf{u}\cdot\mathbf{u}\right)\mathbf{u}d\mathbf{u} = \left(n\mathbf{U} - D\frac{\partial n}{\partial \mathbf{x}}\right)\left(\frac{1}{2}m\mathbf{U}\cdot\mathbf{U} + \frac{5}{2}k_BT\right). \quad (8)$$

Although applicable only in unbounded space far from any wall, this solution can be used nevertheless to construct an approximate boundary condition for the particle number density n of the following form, where f is termed the "particle-flux coefficient" and $\hat{\mathbf{n}}$ is the unit normal vector pointing into the wall and out of the gas:

$$\hat{\mathbf{n}}\cdot\left(n\mathbf{U} - D\frac{\partial n}{\partial \mathbf{x}}\right) = \frac{nc}{\pi^{1/2}}f. \quad (9)$$

This particle-flux boundary condition is analogous to the well-known velocity-slip and temperature-jump boundary conditions [3], in which discontinuities in the tangential velocity and the temperature between a wall and the adjacent gas are taken to be proportional to the shear stress and the heat flux, respectively, and to temperature-jump boundary conditions at a condensing liquid-vapor interface [3]. The particle-flux boundary condition and the advection-diffusion equation, shown below, form a closed system of equations that describes the transport of the particle number density n rather than the particle velocity distribution function N [1]:

$$\frac{\partial n}{\partial t} + \frac{\partial}{\partial \mathbf{x}}\cdot\left(n\mathbf{U} - D\frac{\partial n}{\partial \mathbf{x}}\right) = 0. \quad (10)$$

The particle-flux boundary condition is found by applying the solution for unbounded space at the wall, equating the outgoing portion of the flux to the reflected amount of the incoming portion of the flux, where $R[\mathbf{u}]$ represents the reflection probability,

$$\int_{-\hat{\mathbf{n}}\cdot\mathbf{u}>0} N(-\hat{\mathbf{n}}\cdot\mathbf{u})d\mathbf{u} = \int_{\hat{\mathbf{n}}\cdot\mathbf{u}>0} R[\mathbf{u}]N(\hat{\mathbf{n}}\cdot\mathbf{u})d\mathbf{u}, \quad (11)$$

and rearranging the resulting expression into the form of Eq. (9). The above approach can be applied to the two reflection processes discussed above. The sticking-fraction reflection process has $R[\mathbf{u}]=1-s$ and yields the below expression, where $U=\mathbf{U}\cdot\hat{\mathbf{n}}$ is the normal drift velocity (positive into the wall) and $\hat{U}=U/c$ denotes its normalized value:

$$f = s\left\{2 - s\left(1 + \mathrm{erf}[\hat{U}] - \frac{1-\exp[-\hat{U}^2]}{\pi^{1/2}\hat{U}}\right)\right\}^{-1}. \quad (12)$$

The cutoff-velocity reflection process has

$$R[\mathbf{u}] = \mathrm{H}[\hat{\mathbf{n}}\cdot\hat{\mathbf{u}} - \hat{U}_n]$$

and yields the expression below, where H is the Heaviside function, U_n is the cutoff velocity, $\hat{U}_n=U_n/c$ is its normalized value, and $\hat{U}_d=\hat{U}_n-\hat{U}$:

$$f = \frac{\pi^{1/2}\hat{U}(1-\exp[-\hat{U}_n^2])}{1-\exp[-\hat{U}_n^2]-\exp[-\hat{U}^2]+\exp[-\hat{U}_d^2]+\pi^{1/2}\hat{U}(\mathrm{erfc}[\hat{U}_d]+\mathrm{erfc}[\hat{U}])}. \tag{13}$$

The above expressions exhibit appropriate limiting behavior. When all particles stick ($s=1$ and $\hat{U}_n \to \infty$), these two expressions become identical. In this situation, when $\hat{U}\to\infty$ (infinite drift into the wall), the particle-flux boundary condition becomes $\hat{\mathbf{n}}\cdot(-D\,\partial n/\partial \mathbf{x}) \to 0$, which is an expression commonly used to represent advective outflow for large Peclet numbers. When $\hat{U}\to\infty$ with $s<1$, the particle-flux boundary condition allows exponential decay in the upstream direction (i.e., away from the wall). On the other hand, when $\hat{U}\to-\infty$ (infinite drift away from the wall), the particle-flux boundary condition becomes $n\to 0$, which enforces zero concentration (and hence zero influx) at the wall.

It is convenient to characterize the cutoff-velocity reflection process using the "cutoff parameter" $\sigma=1-\exp[-\hat{U}_n^2]$ in place of the normalized cutoff velocity $\hat{U}_n$. The cutoff parameter σ is similar to sticking fraction s in that $\sigma=1$ ($\hat{U}_n\to\infty$) and $s=1$ both correspond to all particles sticking, and $\sigma=0$ ($\hat{U}_n=0$) and $s=0$ both correspond to all particles reflecting. For an incident half-range Maxwellian, the cutoff fraction equals the sticking fraction; however, when the flux to the wall is nonzero, the incident distribution is not a half-range Maxwellian.

III. LANGEVIN PARTICLE SIMULATIONS

Simulations are performed for particles suspended in a gas in the vicinity of a wall. The gas is taken to be a thermal bath at temperature T, so its molecules are not directly simulated. The stochastic motion of a particle of mass m at position $\mathbf{x}$ with velocity $\mathbf{u}$ is described by the Langevin equation [5,6] with particle drag coefficient β, constant drift velocity $\mathbf{U}$, and random thermal force $\mathbf{X}$ corresponding to the gas conditions at temperature T, which is appropriate when the particle mass is large compared to the gas-molecule mass [7]:

$$m\frac{d\mathbf{u}}{dt} = \beta(\mathbf{U}-\mathbf{u}) + \mathbf{X}, \tag{14}$$

$$\frac{d\mathbf{x}}{dt} = \mathbf{u}. \tag{15}$$

Ermak and Buckholz [6] present an algorithm for integrating the Langevin equation forward in time based on the solution of Chandrasekhar [5] to the generalized Fokker-Planck equation for the distribution function $N[t,\mathbf{x},\mathbf{u}]$ of a particle with velocity $\mathbf{u}_0$ and position $\mathbf{x}_0$ at time t_0 (i.e., an initial distribution function of $N[t_0,\mathbf{x},\mathbf{u}]=\delta[\mathbf{x}-\mathbf{x}_0]\delta[\mathbf{u}-\mathbf{u}_0]$). In particular, they present a method using two independent Gaussian random vectors $\mathbf{B}_1$ and $\mathbf{B}_2$ to advance the particle velocity and position from $\mathbf{u}_0$ and $\mathbf{x}_0$ at time t to $\mathbf{u}$ and $\mathbf{x}$ at time $t+\Delta t$, where $\delta=\exp[-\Delta t/\tau]$:

$$\mathbf{u} = \mathbf{u}_0\delta + \mathbf{U}(1-\delta) + \mathbf{B}_1, \tag{16}$$

$$\mathbf{x} = \mathbf{x}_0 + \tau(\mathbf{u}+\mathbf{u}_0-2\mathbf{U})\left(\frac{1-\delta}{1+\delta}\right) + \mathbf{U}\Delta t + \mathbf{B}_2, \tag{17}$$

$$\langle \mathbf{B}_1\rangle = 0, \quad \langle \mathbf{B}_2\rangle = 0, \quad \langle \mathbf{B}_1\cdot\mathbf{B}_2\rangle = 0, \tag{18}$$

$$\langle \mathbf{B}_1\cdot\mathbf{B}_1\rangle = \frac{3}{2}c^2(1-\delta^2),$$

$$\langle \mathbf{B}_2\cdot\mathbf{B}_2\rangle = 3c^2\tau^2\left\{\frac{\Delta t}{\tau} - 2\left(\frac{1-\delta}{1+\delta}\right)\right\}. \tag{19}$$

The algorithm of Ermak and Buckholz is implemented in an existing molecular-gas-dynamics code that tracks computational molecules which move, reflect from boundaries, and stochastically collide with each other [4,10,11]. This approach takes advantage of the similarity between tracking particles and molecules: the only significant difference is that particles interact with a background fluid rather than colliding with one another. Moreover, the particle-tracking implementation is massively parallel, with good scaling behavior through 10 000 processors, and is therefore capable of simulating billions of particles simultaneously [10,11].

Table I shows the gas and particle parameters used in the Langevin simulations. Spherical PSL particles with a diameter $d=20$ nm suspended in air at a pressure and temperature of $p=101325$ Pa (1 atm) and $T=300$ K are considered, as in recent experiments [2]. The gas-molecule mean free path is defined as $\lambda=\mu/\phi\rho\bar{c}$, where μ is the gas viscosity, $\phi=5\pi/32$ is the mean-free-path constant, $\rho=Mp/k_BT$ is the gas mass density, $\bar{c}=(8k_BT/\pi M)^{1/2}$ is the mean gas-molecule speed, and M is the gas-molecule mass, and the particle Knudsen number is $\mathrm{Kn}=2\lambda/d=6.837$. The drag coefficient is given by $\beta=3\pi\mu d/C$, where the numerator is Stokes drag and the denominator is a slip correction factor of the form $C=1+\mathrm{Kn}(\alpha_s+\beta_s\exp[-\gamma_s/\mathrm{Kn}])$ [1,2]. The experimentally measured values of the three parameters in this expression are used herein [2]. For these conditions, the particle thermal stopping distance is $\ell=\pi^{1/2}D/c=18.13$ nm, which is comparable to the particle diameter.

Table I also shows the numerical parameters used in these simulations. A wall is located at $x=0$, and a particle source is located at $x=L$, where $L=1000$ nm. This domain is divided into cells of width $\Delta x=4$ nm, so the distance between the wall and the particle source is spanned by 250 cells. In these simulations, the only function of the cells is to sample the properties of the particles resident within the cells at each

TABLE I. Simulation parameters (air and PSL).

Quantity	Symbol	Value
Boltzmann constant	k_B	1.380658×10^{-23} J/K
Molecular mass, gas	M	4.811×10^{-26} kg
Pressure, gas	p	101325 Pa
Temperature, gas	T	300 K
Mass density, gas	ρ	1.177 kg/m^3
Molecular mean speed, gas	$\bar{c}$	468.2 m/s
Viscosity, gas	μ	1.85×10^{-5} Pa s
Hard-sphere parameter, gas	ϕ	$5\pi/32\approx0.491$
Mean free path, gas	λ	68.37 nm
Diameter, particle	d	20 nm
Mass density, particle	ς	1050 kg/m^3
Mass, particle	m	4.398×10^{-21} kg
Knudsen number, particle	Kn	6.837
Slip parameter, particle	α_s	1.165
Slip parameter, particle	β_s	0.483
Slip parameter, particle	γ_s	0.997
Drag coefficient, particle	β	2.950×10^{-13} N/(m/s)
Stopping time, particle	τ	14.91 ns
Thermal speed scale, particle	c	1.3724 m/s
Diffusivity, particle	D	1.404×10^{-8} m^2/s
Stopping distance, particle	ℓ	18.13 nm
Domain length	L	1000 nm
Cell size	Δx	4 nm
Time step	Δt	0.5 ns
Steady-state time	t_L	10^6 ns

time step: no spatial "discretization" of the solution occurs. Initially, the domain is devoid of particles. As time progresses, particles enter the domain at a fixed rate from the source (particles attempting to exit the domain at the source are reflected specularly back into the domain), and particles exit the domain at the wall according to one of the two reflection processes discussed above. Time steps of $\Delta t=0.5$ ns are used, and a time of $t_L=10^6$ ns is allowed to pass before sampling is initiated to ensure that steady behavior is established. The average particle number density in each cell is determined by dividing the total number of particles sampled in the cell by the cell volume and by the number of time steps over which sampling is performed. Typical simulations use $\sim10^5$ particles in the domain and sample $\sim10^9$ particles per cell over $\sim10^7$ time steps of steady behavior. Simulations typically require 96 hours on 200 processors of a Linux cluster (i.e., about 2 processor-years).

Figure 1 shows particle-number-density profiles from Langevin simulations for both reflection processes with a zero drift velocity. The profiles are normalized so that the particle number density is unity at the source ($x=L$). Profiles are shown for five values of the sticking fraction s (curves) and the cutoff parameter σ (circles): 0.05, 0.1, 0.2, 0.5, and 1.0. Each cutoff-velocity profile lies slightly above the corresponding sticking-fraction profile except for the case of

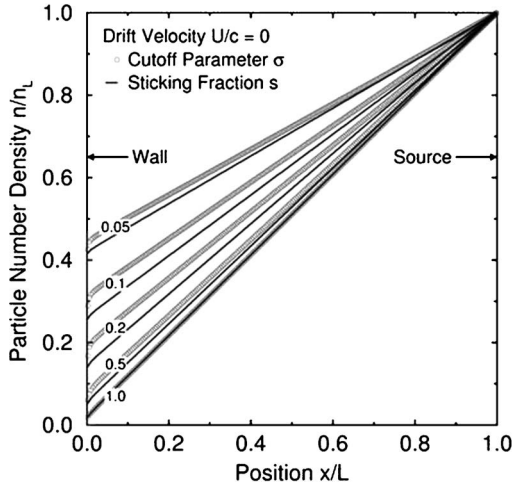

FIG. 1. Particle-number-density profiles from Langevin simulations.

$s=\sigma=1$, for which the two profiles are identical to within the precision of the simulations. All profiles vary linearly with position except near the wall. This near-wall region, located roughly within $0\le x/L<0.1$ ($0\le x<100$ nm, $0\le x/\ell<5$), contains the particle Knudsen layer of each profile. The particle number density adjacent to the wall is nonzero for all profiles.

Figure 2 shows the (near-wall) Knudsen layers for the profiles in Fig. 1. Each Knudsen layer is determined by taking the difference between the actual profile and a straight-line fit through its linear portion (i.e., away from the wall) and subsequently dividing this difference by the slope of the straight-line fit. This slope scaling is performed so that all Knudsen layers are shown at the same particle flux. In all cases except $s=\sigma=1$, the departure of the Knudsen layer from the corresponding straight-line fit is larger for the cutoff-velocity reflection process than for the sticking-fraction reflection process, and the departure increases as the sticking fraction or the cutoff parameter is decreased (i.e., as more particles are reflected by the wall).

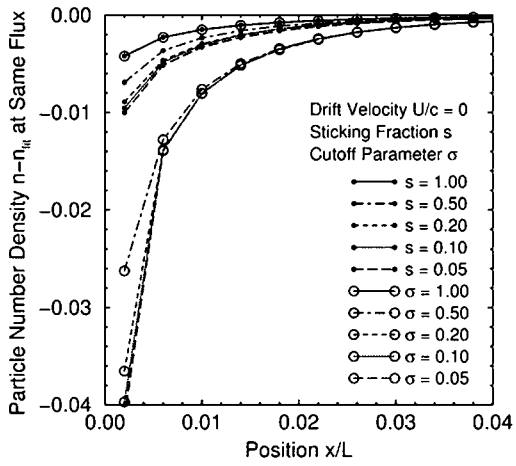

FIG. 2. Particle Knudsen layers from Langevin simulations.

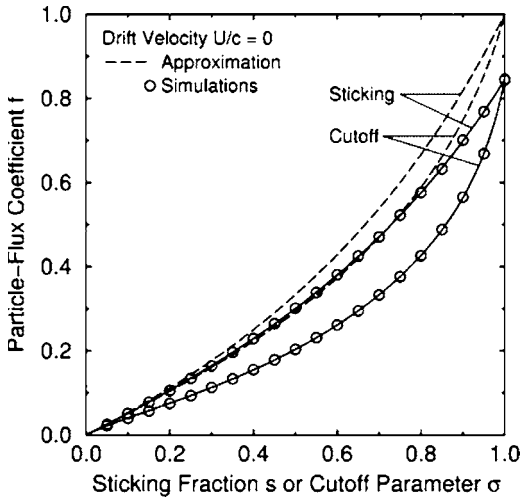

FIG. 3. Particle-flux coefficient for zero drift velocity.

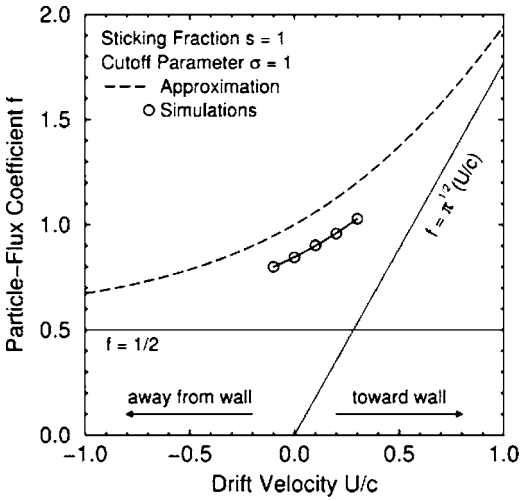

FIG. 4. Particle-flux coefficient for nonzero drift velocities.

IV. COMPARISON OF APPROXIMATION AND SIMULATIONS

Figure 3 shows the particle-flux coefficient f as a function of the sticking fraction s and the cutoff parameter σ for a drift velocity of zero. The particle-flux coefficient is determined in the following manner. A straight-line fit through the linear portion of a profile (i.e., the portion outside the particle Knudsen layer) yields a slope of $(dn/dx)_0$ and an intercept of n_0 at $x=0$. The particle-flux coefficient is found from the particle-flux boundary condition of Eq. (9) according to $f=(\pi^{1/2}D/cn_0)(dn/dx)_0$. The symbols represent the simulation values, and the solid curves connecting the simulation values represent empirically determined correlations that represent the simulation values to ± 0.001 (their uncertainty):

$$f = \left(\frac{s}{2-s}\right)\left(\frac{1+0.506s}{1+0.783s}\right), \tag{20}$$

$$f = \frac{0.5\sigma + 1.665\sigma^2 - 1.843\sigma^3}{1 + 7.412\sigma - 12.456\sigma^2 + 4.426\sigma^3}. \tag{21}$$

The dashed curves in this figure represent the approximations given in Eqs. (12) and (13). The differences between the approximation and the simulation values are modest for the sticking-fraction reflection process but are larger for the cutoff-velocity reflection process. This is not surprising because for the cutoff-velocity reflection process the reflected part of the incoming portion of the particle velocity distribution differs substantially in shape from the outgoing portion. It is noted in passing that the dependence of the particle-flux coefficient f on the sticking fraction s is similar to the dependence of the temperature-jump coefficient f_T on the thermal accommodation coefficient α for Bhatnagar-Gross-Krook gas molecules reflecting from a wall [12]: $f_T \to \alpha/(2-\alpha)$ for $\alpha \to 0$ and $f_T=0.850362$ for $\alpha=1$.

Figure 4 shows the particle-flux coefficient f as a function of the normalized drift velocity $\hat{U}=U/c$ when all particles stick to the wall ($s=\sigma=1$). The symbols represent the simulation results, the dashed curve represents the approximation [Eq. (12)] with $s=1$, and the dotted curves represent the asymptotic behavior of the approximation for large positive or negative values of the drift velocity. The differences between the simulation and approximation values are modest and comparable to those observed in the preceding figure.

V. ADVECTION-DIFFUSION APPLICATION

The utility of the particle-flux boundary condition can be illustrated through an example comparing Langevin particle simulations and advection-diffusion results. The principal advantage of advection-diffusion simulations is that they generally require orders of magnitude less computational effort than that required by particle-based simulation methods [10]. Thus, advection-diffusion simulations are preferred so long as they are accurate.

A paradigmatic geometry often encountered in real systems (e.g., particle contamination in semiconductor manufacturing) involves two infinite parallel horizontal solid plates separated by a distance L, where the gap between the plates is filled with motionless gas at conditions that are nearly independent of time and position. Particles with an equilibrium velocity distribution are placed at a distance H above the lower plate (denoted "1") and thus a distance $L-H$ below the upper plate (denoted "2"). An advection-diffusion analysis using Eqs. (9) and (10) yields the probabilities P and $1-P$ that particles deposit on the upper and lower plates, respectively, where the drift velocity U is positive when pointing downward (i.e., from plate 2 to plate 1) and the arrow denotes the zero-drift-velocity limit:

$$e_H = \exp[HU/D], \quad e_L = \exp[LU/D], \tag{22}$$

$$\hat{V} = \pi^{1/2}U/c, \quad \ell = \pi^{1/2}D/c, \tag{23}$$

$$P = \frac{f_2[(e_H - 1)f_1 + \hat{V}]}{(e_L - 1)f_1 f_2 + (e_L f_1 + f_2)\hat{V}}, \tag{24}$$

$$P \to \frac{f_2 \ell + f_1 f_2 H}{(f_1 + f_2)\ell + f_1 f_2 L}. \tag{25}$$

In the further limit that the thermal stopping distance vanishes ($\ell/L \to 0$), the zero-drift-velocity probability reduces to the well-known expression H/L.

Rather than placing particles at a particular height, an ensemble of particles is injected vertically upward from the lower plate at a velocity U_I and comes to rest at a height $H = U_1 \tau$ above the lower plate. This height is used in the advection-diffusion expressions above. However, if this height exceeds the plate separation L, a fraction s_2 of the particles sticks to the upper plate, and the remaining fraction is specularly reflected downward and comes to rest at a height $H = 2L - U_I \tau$. In this circumstance, this new height is used in Eqs. (22)–(25), but the probability of deposition on the upper plate becomes $s_2 + (1 - s_2)P$. If this new height lies below the lower plate, a fraction s_1 sticks to the lower plate, the remaining fraction is reflected specularly upward, the deposition probability is correspondingly modified, and so forth.

Langevin particle simulations are performed for the above situation and compared with Eqs. (22)–(25). The gas is nitrogen at 295 K and 6.666 Pa (50 mtorr), the particles have a mass density of 1000 kg/m^3, and the slip-correction parameters are $\alpha_s = 1.207$, $\beta_s = 0.440$, and $\gamma_s = 0.78$ [2]. A plate separation of 1 cm and an injection velocity of 10 m/s are considered. Two sets of simulations are performed. In the first set, the sticking fraction on both plates is $s = 1$, but the downward gravitational acceleration is varied within the range 0-10g, where $g = 9.81$ m/s^2. Thus, this set of simulations contains cases with zero and nonzero drift velocities since $U = mg/\beta$. In the second set, the gravitational acceleration is maintained at a value of g, but the sticking fraction on both plates is one of three values: $s = 1$, 0.1, 0.01.

Figures 5 and 6 show the deposition probability from the two simulation sets above. The symbols represent the values from the Langevin particle simulations, and the curves represent the values from the advection-diffusion expressions. Since a nonzero drift velocity is present in most of these cases, the particle-flux coefficients in the advection-diffusion expressions are evaluated using Eq. (12). In all cases, the agreement is excellent. In particular, this includes the cases in which the sticking fraction is not unity. For these cases, the commonly used zero-particle-number-density boundary condition would produce values close to the $s = 1$ values in Fig. 6, which differ greatly from the actual values. It is noted in passing that nonmonotonic variations of aerosol quantities with particle diameter typically occur because of the transition from free-molecular gas flow for small particles to continuum gas flow for large particles [1].

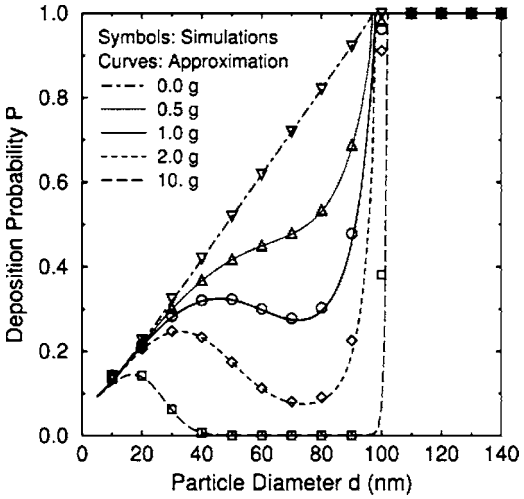

FIG. 5. Effect of gravity on deposition probability.

VI. CONCLUSIONS

The above theoretical and numerical investigation indicates that the particle number density of a nanoparticle aerosol tends to a nonzero value at a solid boundary (a wall) and that this value is proportional to the flux to the wall and depends upon the reflection process. A methodology is presented that enables an approximate advection-diffusion boundary condition to be determined for arbitrary reflection processes. Although developed for a flat surface, this boundary condition can be used for a nonflat surface so long as its radius of curvature is large compared to the thickness of the particle Knudsen layer (corners do not satisfy this restriction). The accuracy of advection-diffusion simulations using this boundary condition can be quantified by comparison to corresponding Langevin particle simulations.

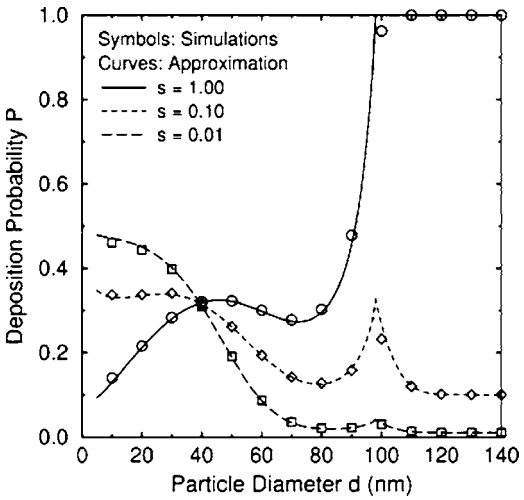

FIG. 6. Effect of sticking fraction on deposition probability.

ACKNOWLEDGMENTS

This work was performed at Sandia National Laboratories. Sandia is a multiprogram laboratory operated by Sandia Corporation, a Lockheed Martin Company, for the United States Department of Energy's National Nuclear Security Administration under Contract No. DE-AC04-94AL85000. The authors gratefully acknowledge financial support from Intel Corporation under CRADA SC93/01154 and technical interactions with Kevin J. Orvek, David Y. H. Pui, Christof Asbach, and Heinz Fissan.

[1] S. K. Friedlander, *Smoke, Dust, and Haze: Fundamentals of Aerosol Dynamics*, 2nd ed. (Oxford, New York, 2000).

[2] J. H. Kim, G. W. Mulholland, S. R. Kukuck, and D. Y. H. Pui, J. Res. Natl. Inst. Stand. Technol. **110**, 31 (2005).

[3] C. Cercignani, *Rarefied Gas Dynamics: From Basic Concepts to Actual Calculations* (Cambridge University Press, Cambridge, 2000), Chap. 8.

[4] G. A. Bird, *Molecular Gas Dynamics and the Direct Simulation of Gas Flows* (Clarendon, Oxford, 1994).

[5] S. Chandrasekhar, Rev. Mod. Phys. **15**, 1 (1943).

[6] D. L. Ermak and H. Buckholz, J. Comput. Phys. **35**, 169 (1980).

[7] J. J. Brey, J. W. Dufty, and A. Santos, J. Stat. Phys. **97**, 281 (1999).

[8] B. Dahneke, J. Colloid Interface Sci. **37**, 342 (1971); **45**, 584 (1973); **51**, 58 (1975).

[9] J. Happel and H. Brenner, *Low Reynolds Number Hydrodynamics* (Martinus Nijhoff, The Hague, 1983).

[10] M. A. Gallis, D. J. Rader, and J. R. Torczynski, Phys. Fluids **13**, 3482 (2001).

[11] M. A. Gallis, D. J. Rader, and J. R. Torczynski, American Institute of Aeronautics and Astronautics, Reston, Report No. AIAA-2002-2760, 2002.

[12] C. E. Siewert, J. Quant. Spectrosc. Radiat. Transf. **77**, 417 (2003).